JOURNAL OF PROPULSION AND POWER
Vol. 18, No. 6, November–December 2002

Motor and Plume Particle Size Prediction in Solid-Propellant Rocket Motors

Oleg B. Kovalev*
Russian Academy of Sciences, 630090, Novosibirsk, Russia

Models are developed for 1) agglomeration of powdered aluminum on the burning surface of a metallized composite solid propellant in order to predict average diameter of aluminum agglomerates as a function of propellant composition, pressure, burning rate, and size distribution of oxidizer particles and 2) the processes of coagulation and aerodynamic shattering of liquid aluminum-oxide droplets in an accelerating gas flow. The critical upper value of droplet diameter in the throat, which is calculated theoretically, is in agreement with the mean-mass diameter D_{43} obtained by numerical simulation of a two-phase flow with coagulation and particle breakup. A formula is proposed for the average particle diameter at the nozzle exit, which is confirmed by agreement with the measured values of D_{43} of aluminum-oxide particles in plumes of small, medium-sized, and large solid rocket motors. The proposed formula is also in agreement with Hermsen's correlation of measured diameters. Based on a comparison between theoretical calculations and numerous experimental data, the formula is recommended for prediction of the aluminum-oxide particle size in plumes of various types of solid rocket motors.

Nomenclature

c	=	specific heat capacity
c_p	=	specific heat capacity of the gas at constant pressure
D	=	diameter
E	=	activation energy
F	=	cross-sectional area
K	=	preexponent
k	=	ratio of specific heats
Le	=	$\lambda_g/(\rho_g \kappa_g c_p)$, Lewis number
m	=	mass
Nu	=	Nusselt number
P	=	pressure
Pr	=	Prandtl number
Q	=	heat of reaction
R	=	radius
R^0	=	universal gas constant [8.31441 J/(K mole)]
Re	=	$(1-\alpha_{\mathrm{Al}})\rho_T \omega \delta_a/\mu_g$, Reynolds number
S	=	elementary surface of a fuel-binder
T	=	temperature
t	=	time
W	=	$\rho_a w_a/\rho_g w_g$, particle/gas fraction
We	=	$\rho_g(w_g - w_a)/\sigma_b$, Weber number
w	=	velocity
x, y, z	=	coordinates
Y	=	mass concentration of the gas
α	=	mass fraction
β	=	volume fraction
γ	=	reduced velocity
δ	=	agglomerate diameter
ε	=	emissivity
η	=	oxide-film thickness
κ	=	diffusion coefficient
λ	=	thermal conductivity
μ	=	viscosity
ν	=	stoichiometric coefficient
ρ	=	density
σ	=	surface tension
σ_0	=	5.67×10^{-8} W/(m^{2}K^4), Stefan–Boltzmann radiation constant
τ	=	dimensionless temperature
χ	=	molecular weight
ω	=	composite solid propellant burning rate

Subscripts

a	=	"aggregate," agglomerate
Al	=	aluminum
agl	=	lifted-off agglomerate
b	=	material
C	=	curvature
e	=	equilibrium
f	=	polymeric binder
g	=	gas
j	=	number of the fraction of oxidizer particles or pocket number
ox	=	oxidizer
s	=	surface
T	=	solid propellant
t	=	throat value
1	=	gaseous oxidizer
2	=	gaseous propellant
3	=	gaseous products of reaction
∞	=	gas-phase flame
$\sim$	=	quantity averaged over the diameter δ:

$$\left[\tilde{T} = \frac{1}{\delta}\int_0^{\delta} T(z)\,\mathrm{d}z\right]$$

Received 3 January 2002; revision received 26 April 2002; accepted for publication 22 May 2002.

*Professor, Physics of Fast Processes Laboratory, Institute of Theoretical and Applied Mechanics.

I. Introduction

COMBUSTION of composite solid propellants (CSPs) is accompanied by accumulation and agglomeration of aluminum particles on the reacting surface. According to the estimates of previous investigations,[1–7] the diameter of particles ejected from the surface by gaseous products of CSP decomposition can vary from 5–10 to 200–800 μm. The absence of prediction and control over the degree of agglomeration can result in undesirable deposition of burning particles onto walls in the combustion chamber and motor malfunctions. The existing analytical models[8–12] cannot predict the size distribution function of particle agglomerates leaving the

burning surface, which is vitally necessary for numerical simulation of two-phase flow in the chamber. Among well-known models are those reported in Refs. 10 and 11, which are based on the pocket model of agglomeration. According to this model, the volume between ammonium perchlorate (AP) particles provides isolated pockets in which the accumulation and interaction of particles occur with the binder and small aluminum particles; as a result, particle agglomerates are formed with dimensions limited by the pocket sizes and the content of aluminum in them. The pocket model of agglomeration is widely used in analysis of CSP burning. Correlations of agglomerate diameter on the volume of pocket and AP particle sizes, which are similar in shape, are analyzed in Refs. 6, 13, and 14. Unfortunately, the pocket model ignores the effect of pressure in the combustor, the changes in the burning rate, etc. In addition, the study[5] shows that, apart from the pocket model of agglomeration, there are interpocket mechanisms (where agglomerates of different pockets merge) and prepocket mechanisms (where more than one agglomerate is formed in the pocket). Agglomeration of aluminum depends on many competitive dynamic processes; the lack of knowledge of these processes leads to insoluble difficulties in the agglomeration description. It follows from the analysis that the agglomeration models developed should be rigidly related to CSP composition and the character of its burning.

Being located on the surface or close to it, particle agglomerates have enough time to ignite. A two-phase flow with liquid burning polydisperse particles is formed in the combustor. Having different particle-gas lag, the particles might collide with each other and interact. Particularly large agglomerates entrained by the gas flow can break as a result of the Rayleigh–Taylor instability arising in them. Combustion of metal particles in the chamber proceeds at a temperature of the ambient gas ~3000–3500 K and is accompanied by the formation of condensed aluminum oxide; therefore, when aluminum burns out its oxide in the liquid form remains on the agglomerate. This indicates that particle agglomerates, entering the flow and traversing the distance from the burning surface to the nozzle, cannot change significantly their diameters caused by combustion. Even in the case of complete oxidation of aluminum, particle agglomerates change in diameter by only 20–40% (Ref. 14).

Historically, models of the motion of two-phase mixtures were based on experimental studies of solid rocket motor (SRM) nozzle flows.[15–24] Models of two-phase flows[15] were initially constructed on the assumption that the particle size is small (~1–2 μm), their volume concentration is insignificant ($<10^{-4}$), and the particles exert no effect on the gas and do not interact with each other. The gas played a role of a carrier phase, which activity was reduced to resisting strength stipulated viscosity of gas and friction at streamlining a particle. The influence of volume of particles and constraint of a stream[16] was complicated by equations of motion; the type of these equations became composite,[25] which have complicated the mathematical statement of boundary-value problems. Models of polydisperse two-phase flows were proposed to take into account particle interaction, which allowed calculation of particle growth as a result of collisions and coagulation.[17–20] These models were later complemented in Refs. 21–23 by a description of fragmentation effects during collisions.

One of the main principles of mechanics of heterogeneous media[26] is the condition of conservation of nesting of mixture scales. In other words, the characteristic scale on which the averaged flow parameters change significantly should be much greater than the scale of nonuniformity, that is, particle size. Thus, the assumption of the small particle size is the most severe requirement in all models of two-phase flows, and it is impossible to avoid it.

The most important factor that suppresses significantly the growth of particles is their aerodynamic fragmentation caused by interaction with the gas flow. Aerodynamic fragmentation of liquid particles is described by the dimensionless Weber criterion, which characterizes the ratio of the aerodynamic and surface tension forces on the particle. The Weber criterion of fragmentation allows two-phase flow theory to satisfy the scale principle.

Hermsen[27] documents an extensive bibliography of the previously published experimental data on the measured mean-mass particle diameter D_{43} in plumes of a large number of various SRMs, which differ in size, propellant type, content of aluminum, nozzle geometry, etc. He also lists a number of empirical dependences obtained by the least-squares method for D_{43}. According to the data of Ref. 27 D_{43} for the selected Al_2O_3 particles at the nozzle exit is in the range $0.25 \le D_{43} \le 13.3$ μm.

Laredo et al.[28] present the results of measurements of aluminum agglomerate dimensions not only at the nozzle exit but also in combustion chambers of very small-scale engines with channel and head-end combustion. Observation and optical measurement of particles in the combustor were performed through a special window built into the engine body. The window was mounted either ahead of the nozzle entrance or near the propellant surface. According to Ref. 28, aluminum agglomerates leaving the propellant surface at a pressure of 3.6 MPa had the normallogarithmic size distribution with a mean volume-surface diameter $D_{32} = 132$ μm and standard deviation of 18 μm and were significantly greater than the initial aluminum powder in the propellant. Almost all large agglomerates turned into a large number of small particles as they moved along the combustor. The mass concentration of small particles ($D_{32} < 2$ μm) at the nozzle exit was less than 10%, most particles had $D_{32} < 50$ μm, and only a small number of particles had $D_{32} > 85$ μm. The mean volume-surface diameter D_{32} at the nozzle exit was less than 2.5 μm.

A joint analysis of the results of numerous experimental studies[27,28] and numerical simulations[17–24,29] of polydisperse two-phase flows with liquid particles in SRM nozzles yields the following pattern of variation of the granulometric composition of particles in the two-phase flow. The mean-mass diameter $D_{43}(x)$ as a function of the x coordinate exhibits the greatest change in the subsonic part of the nozzle, including the throat. If small particles are injected at the nozzle entrance [$D_{43}(0) = 0.01$–2 μm], then the calculations of Refs. 17–19 yield a monotonic increase in $D_{43}(x)$ for $x > 0$, which is sustained by coagulation caused by collisions of particles with each other because of the difference in the velocity lag relative to the gas. The conditions of aerodynamic fragmentation according to the Weber criterion $We \ge We_t$ for particles of this size either cannot be reached at all or are fulfilled for individual large fractions. Effects of breakup as a result of collisions can be manifested very seldom and for individual particles only. If large particles are injected at the nozzle entrance [$D_{43}(0) = 20$–100 μm], the curve of $D_{43}(x)$ has alternating sectors of monotonic increase and drastic decrease, which are caused by particle breakup induced by reaching the critical conditions of aerodynamic fragmentation $We \ge We_t$. The effect of aerodynamic fragmentation prevails over coagulation, and the dependence $D_{43}(x)$ decreases with increasing x.

Behind the throat, the expanding flow is stratified so that large fractions of particles remain in the core of the stream (as a result of inertia), whereas small particles have enough time to change their trajectory to follow the gas and are deflected toward the nozzle wall. Under these conditions the lag between the gas and particle velocities becomes small, and $D_{43}(x)$ remains almost unchanged.[17,18,23,29]

An analysis of specially performed calculations Kovalev and Fomin[29] shows that, as a result of aerodynamic fragmentation and coagulation of particles, the mean-mass diameter $D_{43}(x)$ of particles in an accelerating gas flow tends to a limiting value, which is reached in the nozzle throat and then remains almost unchanged up to the nozzle exit. Under these conditions the regime of the flow around liquid droplets always remains close to the Stokes law ($C_x = 24/Re$). A deviation from this law inevitably leads to the development of the Rayleigh–Taylor instability inside the particle. Under conditions of rapid acceleration of the gas flow, particularly in the subsonic part of the nozzle, instability occurs almost instantaneously, which leads to particle breakup. Unfortunately, quantitative characteristics of fragmentation (number and size) of the droplets formed cannot be rigorously described. Thus, liquid droplets of Al or Al_2O_3 suffer the greatest changes in size during their motion through the engine nozzle.

In the present work a numerical-analytical analysis of aluminum agglomeration processes on the CSP burning surface is performed,

and the degree of shattering and coagulation of liquid Al_2O_3 droplets in SRM nozzles is evaluated.

II. Aluminum Agglomeration Model

In constructing the physical model of aluminum agglomeration, we will use experimental results available in this field,[3–5] where the most typical features of the formation of aluminum agglomerates in combustion of AP-based model CSPs with moderate content of metal are formulated. The main assumptions on which the model is based are as follows (see Fig. 1):

1) The CSP burning surface, following Ref. 30, is assumed to consist of cells including elementary surfaces of the AP oxidizer and the polymeric binder with small (diameter $\delta_s = 5$–$15\ \mu$m) particles of aluminum.

2) In the course of decomposition of the binder, accumulation of aluminum particles occurs within the surface S bounded by AP grains.

3) The initial aluminum particles that appear on the surface S have a temperature equal to the burning surface temperature ($T_s = 800$–1000 K), that is, higher than the aluminum melting point and lower than the aluminum-oxide melting point.

4) Within the surface S an "aggregate" consisting of contacting aluminum particles is initially formed; cohesion of particles is ensured either through carburizing by carbon-containing products of polymer decomposition or by liquid aluminum that appears partly on the particle surface, which results from the formation of cracks on the oxide film.

5) The shape of the aggregate is such that it is always possible to introduce some effective diameter $\delta_a(t)$ and effective width of the oxide film $\eta_a(t)$.

6) There is no temperature gradient inside the aggregate, which allows us to introduce the mean temperature $T_a(t)$ over the mean diameter $\delta_a(t)$ of the aggregate.

7) The aggregate is affected by the general confining mechanical force (surface tension and other forces), which retains it on the surface S, the body force, and the Stokes drag force induced by the flux of gases formed by decomposition of the polymeric propellant.

8) If the aggregate is small (δ_a less than 500 μm), the mass force is also small and can be ignored.[5]

9) The internal energy of the aggregate changes as a result of heat exchange with the ambient gas q_c, radiant flux q_r from the diffuse-kinetic flame, internal self-heating resulting from aluminium oxidation, and contact interaction with colder particles.

10) The aggregate increases in size until the moment of aluminum ignition, after which the initial particles merge and form a spherical agglomerate; at this moment the confining mechanical relation with the surface is broken, and the agglomerate hangs above the surface and is entrained by the gas flow under the action of the Stokes force.

11) The geometric configuration of the propellant surface remains "frozen," that is, S remains unchanged in time up to complete formation and separation of the agglomerate (see Fig. 1).

A. Laws of Conservation

The variation of the mass and internal energy of the aggregate (agglomerate) is described by the following system:

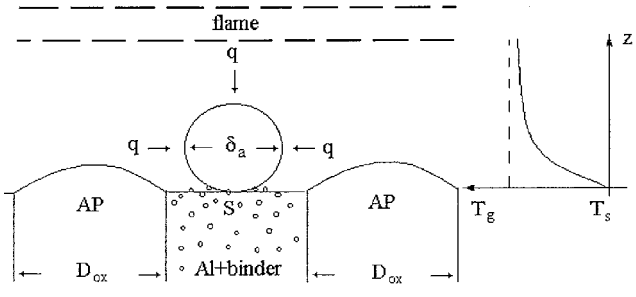

Fig. 1 Aluminum agglomeration model.

$$\frac{\mathrm{d}}{\mathrm{d}t}m_a = \beta_{\mathrm{Al}}\rho_{\mathrm{Al}}\omega_T S, \qquad m_a = \frac{\pi}{6}\rho_{\mathrm{Al}}\delta_a^3 \tag{1}$$

$$\frac{\mathrm{d}}{\mathrm{d}t}(m_a c_{\mathrm{Al}} T_a) = c_{\mathrm{Al}} T_s \frac{\mathrm{d}m_a}{\mathrm{d}t} + \pi\delta_a^2\left(q + Q_a\frac{\mathrm{d}\eta_a}{\mathrm{d}t}\right) \tag{2}$$

$$\frac{\mathrm{d}}{\mathrm{d}t}\eta_a = \frac{K_a}{\eta_a}\exp\left(-\frac{E_a}{R^0 T_a}\right) \tag{3}$$

$$t = 0: \quad T_a = T_s, \qquad \eta_a = \eta_s, \qquad \delta_a = \delta_s$$

$$q = q_c + q_r, \qquad q_c = \frac{\lambda_g Nu}{\delta_a}(\tilde{T}_g - T_a)$$

$$q_r = \varepsilon_0\sigma_0\left(T_\infty^4 - T_a^4\right), \qquad \varepsilon_0 = \frac{1}{1/\varepsilon_a + 1/\varepsilon_g - 1}$$

The functions $\delta_a(t)$, $T_a(t)$, and $\eta_a(t)$ are unknown quantities. The first equation describes the change in the aggregate mass as a result of addition of initial aluminum particles from the heated layer. The second equation describes the energy balance of the aggregate, and the third equation is the effective law of oxidation for the conglomerate of aluminum particles.[31]

The CSP composition determines completely the size of elementary surfaces of the oxidizer and fuel-binder.[30] According to Ref. 32, we can write $S = \pi D_{\mathrm{ox}}^2(1-\beta_{\mathrm{ox}})/6\beta_{\mathrm{ox}}$; here D_{ox}, β_{ox} are the mean diameter and the volume fraction of the oxidizer particles.

To calculate heat exchange between the agglomerate and gaseous products of decomposition around it, we use the following expression for the Nusselt number[26]:

$$Nu = \begin{cases} 2 + 0.5RePr, & Re \le 1 \\ 2 + 0.46Re^{0.55}Pr^{0.33}, & Re > 1 \end{cases} \tag{4}$$

Here $Pr = c_p\mu_g/\lambda_g$ is the Prandtl number, and $Re = \rho_g v_g \delta_a/\mu_g \approx (1-\alpha_{\mathrm{Al}})\rho_T\omega_T\delta_a/\mu_g$ is the Reynolds number.

The growth of an agglomerate begins with a diameter δ_s of initial particles Al, which have width of an oxide film η_s. The final diameter of an agglomerate, which is carried out in a stream, is determined then, when its temperature $T_a(t)$ begins unrestrictedly to increase: $T_a(t) \to \infty$, $\delta_a(t) \to \delta_{\mathrm{agl}}$. Equations (1–3) for the first time were offered in Ref. 33, but without the account radiant component q_r of heat exchange between an agglomerate and gas, which, as will be shown next, essentially influences on its heat-up.

Equation (1) is immediately integrated, whence $\delta_a(t) = \delta_s[1 + (6\beta_{\mathrm{Al}}\omega_T S/\pi\delta_s^2)t]^{1/3}$. After transition to dimensionless variables and elimination of time, two other equations [(2) and (3)] are reduced to the following form:

$$\frac{\mathrm{d}}{\mathrm{d}x}\Theta = \Omega\Lambda\frac{x}{1+\mathrm{Z}}\exp\left(\frac{\Theta}{1+\Delta\Theta}\right) + \Sigma\Theta_g - \left(\frac{3}{x} + \Sigma\right)\Theta$$
$$+ \mathrm{E}x\left[(1+\Delta\Theta_\infty)^4 - (1+\Delta\Theta)^4\right] \tag{2*}$$

$$\frac{\mathrm{d}}{\mathrm{d}x}\mathrm{Z} = \Lambda\frac{x^2}{1+\mathrm{Z}}\exp\left(\frac{\Theta}{1+\Delta\Theta}\right) \tag{3*}$$

$$x = x_s, \qquad \Theta = 0, \qquad \mathrm{Z} = 0$$

$$\Theta = \frac{E_a}{R^0 T_s^2}(T - T_s), \qquad Z = \frac{\eta - \eta_s}{\eta_s}, \qquad x = \frac{\delta_a}{D_{\mathrm{ox}}}$$

$$\Omega = \frac{6}{\Delta}\frac{Q_a}{\rho_{\mathrm{Al}}c_{\mathrm{Al}}T_s}\frac{\eta_s}{D_{\mathrm{ox}}}, \qquad \Lambda = \frac{\pi K_a}{2\beta_{\mathrm{Al}}\omega_T S}\frac{D_{\mathrm{ox}}^3}{\eta_s^2}\exp\left(-\frac{1}{\Delta}\right)$$

$$\Sigma = \frac{3\pi\lambda_g D_{\mathrm{ox}}}{c_{\mathrm{Al}}\rho_{\mathrm{Al}}\beta_{\mathrm{Al}}\omega_T S}Nu, \qquad \mathrm{E} = \frac{3\pi}{\Delta}\frac{D_{\mathrm{ox}}^2\varepsilon_0\sigma_0 T_s^3}{c_{\mathrm{Al}}\rho_{\mathrm{Al}}\beta_{\mathrm{Al}}\omega_T S}$$

$$S = \frac{\pi D_{\mathrm{ox}}^2(1-\beta_{\mathrm{ox}})}{6\beta_{\mathrm{ox}}}, \qquad \Delta = \frac{R^0 T_s}{E_a}$$

Here x is the dimensionless diameter; $\Theta(x)$ is the dimensionless temperature, and $\mathrm{Z}(x)$ is the dimensionless effective width of the oxide film of the agglomerate.

B. Calculation of the Heat-Wave Profile in the Gas

According to the commonly accepted notions,[30] the products of decomposition of the oxidizer and fuel-binder react with each other and form local microflames (kinetic and diffuse ones). The kinetic microflame arises at a certain distance from the solid surface and is characterized by combustion of the premixed mixture of gaseous oxidizer and fuel-binder. In the diffuse microflame the oxidizer and propellant are separated so that combustion is limited to diffusion of components to the reaction zone. According to the Beckstead Derr Price (BDP) model,[30] diffuse microflames arise in regions of stoichiometric ratios of the components. If the propellant composition is overrich in the binder, the surfaces of stoichiometric ratios of the components merge above the oxidizer particles and have a paraboloid shape. The formation of a kinetic microflame on the stoichiometric surface of the components leads to the appearance of a diffuse microflame. Thus, at low pressures the kinetic microflame can cross only the tips of stoichiometric surfaces above large particles of the oxidizer,[4] on which diffuse microflames are formed. With increasing pressure the stand-off distance of the kinetic microflame from the solid surface decreases, and diffuse microflames can be formed on finer fractions of the oxidizer. Heating and ignition of agglomerates is accelerated as a result of interaction with microflames.[4] Thus, the position of the kinetic microflame is a factor that hampers the growth of particles and limits the degree of agglomeration.

Solving the problem of CSP burning in the general case is currently rather problematic. We consider a simplified formulation of the problem. It is assumed that the chemical processes in the flame are irreversible and proceed in one stage $\nu_1 A_1 + \nu_2 A_2 = \nu_3 A_3$ with velocity $\Psi(Y_1, Y_2, T_g)$. The presence of aluminum particles and agglomerates on the surface does not exert a significant effect on the formation of microflames. The distance at which the kinetic microflame is formed is determined by solving one-dimensional equations of heat conduction and diffusion of the components[34] (see Fig. 1):

$$c_p m_T \frac{\mathrm{d}}{\mathrm{d}z} T_g - \lambda_g \frac{\mathrm{d}^2}{\mathrm{d}z^2} T_g = Q_g \Psi(Y_1, Y_2, T_g) \tag{5}$$

$$m_T \frac{\mathrm{d}}{\mathrm{d}z} Y_1 - \rho_g \kappa_g \frac{\mathrm{d}^2}{\mathrm{d}z^2} Y_1 = -\nu_1 \chi_1 \Psi(Y_1, Y_2, T_g) \tag{6}$$

$$m_T \frac{\mathrm{d}}{\mathrm{d}z} Y_2 - \rho_g \kappa_g \frac{\mathrm{d}^2}{\mathrm{d}z^2} Y_2 = -\nu_2 \chi_2 \Psi(Y_1, Y_2, T_g) \tag{7}$$

$$z = 0: \quad T_g = T_s, \qquad Y_1 = Y_{1s} = \frac{\alpha_{\mathrm{ox}}}{1 - \alpha_{\mathrm{Al}}}$$

$$Y_2 = Y_{2s} = 1 - \frac{\alpha_{\mathrm{ox}}}{1 - \alpha_{\mathrm{Al}}}$$

$$z = +\infty: \quad T_g = T_\infty, \qquad Y_1 = Y_{1\infty}, \qquad Y_2 = Y_{2\infty}$$

$$\Psi = K_g \left(\frac{Y_1 P}{R^0 T_g}\right)^{\nu_1} \left(\frac{Y_2 P}{R^0 T_g}\right)^{\nu_2} \exp\left(-\frac{E_g}{R^0 T_g}\right) \tag{8}$$

If the first component (oxidizer) is deficient in the CSP, then $Y_{1\infty} = 0$, $Y_{2\infty} \neq 0$; otherwise, $Y_{1\infty} \neq 0$, $Y_{2\infty} = 0$. The z coordinate changes along the normal to the solid surface of the propellant.

Assuming that the Lewis number is $Le = \lambda_g / \rho_g \kappa_g c_p = 1$, system (5–8) reduces to one equation in dimensionless variables[34]:

$$\frac{\mathrm{d}}{\mathrm{d}h}\tau - \frac{\mathrm{d}^2}{\mathrm{d}h^2}\tau = \frac{\lambda_g Q_g E_g}{m_T^2 c_p^2 R^0 T_\infty^2} \Psi(\tau)$$

$$h = 0: \quad \tau = \tau_s, \qquad h = +\infty: \quad \tau = 0$$

$$h = \frac{c_p m_T}{\lambda_g} z, \qquad \tau = \frac{E_g}{R^0 T_\infty^2}(T_g - T_\infty) \tag{9}$$

To solve Eq. (9), we use an approximate integral method with temperature approximated by the third-order polynomial

$$\tau = \tau_s [1 - 1.5(h/H) + 0.5(h/H)^3] \tag{10}$$

where the coefficients are determined from the boundary conditions

$$h = 0: \quad \tau = \tau_s, \qquad \frac{\mathrm{d}^2}{\mathrm{d}h^2}\tau = 0$$

$$h = H: \quad \tau = 0, \qquad \frac{\mathrm{d}}{\mathrm{d}h}\tau = 0$$

Equation (10) represents the variation of gas temperature across the layer from the propellant surface to the flame. Here H is the dimensionless thickness of the thermal boundary layer or the distance at which the kinetic microflame is formed. Setting additional boundary conditions on the derivatives is a natural requirement in the theory of the stationary thermal boundary layer. Substituting Eq. (10) into Eq. (9) and integrating with respect to h from 0 to H, we obtain a quadratic equation for H; solving it, we find

$$H = \frac{\Phi + \sqrt{\Phi^2 + 6\Phi}}{2}$$

$$\frac{1}{\Phi} = -\frac{\lambda_g Q_g E_g K_g Y_{1s}^{\nu_1} Y_{2s}^{\nu_2}}{\tau_s R^0 T_\infty^2 (c_p m_T)^2} \left(\frac{p}{R^0 T_\infty}\right)^{\gamma_0} \exp\left(-\frac{1}{\Delta_g}\right) \int_0^1 \Psi[\tau(Ht)]\,\mathrm{d}t$$

$$\Psi = \left(\frac{\tau}{\tau_s}\right)^{\nu_1} \left[1 - \frac{Y_{1s}}{\nu Y_{2s}}\left(1 - \frac{\tau}{\tau_s}\right)\right]^{\nu_2} \frac{\exp[\tau/(1 + \Delta_g \tau)]}{(1 + \Delta_g \tau)^{\nu_0}}$$

$$\nu_0 = \nu_1 + \nu_2, \qquad \nu = \frac{\nu_1 \chi_1}{\nu_2 \chi_2}, \qquad \Delta_g = \frac{R^0 T_\infty}{E_g}$$

Within the range $0 \le t \le 1$, τ varies from 0 to $\tau_s < 0$. We can easily see that $\Psi(\tau) \ge 0$ across the layer $\tau_s \le \tau < 0$ and is limited by the condition $Y_{1s}/\nu Y_{2s} \le 1$, which corresponds to lack of the oxidizer. Equations (5–9) assume that the mass burning velocity $m_T = \rho_T \omega_T$ is known (Moreover, the dependence of the burning rate on pressure is also known.), which allows one to calculate the parameters at $+\infty$. In particular, for the burning temperature T_∞, we obtain $T_\infty = T_s + (Q_g/c_p)[Y_{1s} Y_{2s}/(\nu_1 Y_{2s} + \nu_2 Y_{1s})]$. The calculation of the gas temperature profile $T_g(z)$ begins from estimating T_∞, then Φ and H are determined at a given pressure p, and, finally, $\tau(h)$ and $T_g(z)$ are found (Fig. 1).

C. Calculation of the Effective Diameter of Agglomerates Lifting Off from the Surface *S*

Introducing the effective temperature of the gas on the agglomerate surface by the formula

$$\tilde{T}_g = \frac{1}{\delta_a} \int_0^{\delta_a} T_g(z)\,\mathrm{d}z$$

we provide mathematical closure. Integration of Eqs. (1–3) was performed by the fourth-order Runge–Kutta method with a variable step. The following values of constant parameters were used in calculations: $T_s = 980$ K, $\delta_s = 15.0 \times 10^{-6}$ m, $\eta_s = 5 \times 10^{-7}$ m, $\lambda_g = 0.1258$ J/(m·s·K), $\mu_g = 7.2 \times 10^{-5}$ N·s/m^2, $c_p = 1257$ J/(kg·K), $\nu_1 = 1$, $\nu_2 = 1$, $c_{\mathrm{Al}} = 1000$ J/(kg·K), $\rho_{\mathrm{Al}} = 2000$ kg/m^3, $\chi_1 = 27.893$ kg/kmole, and $\chi_2 = 30$ kg/kmole. The law of oxidation of a conglomerate of aluminum particles was borrowed from Ref. 31: $E_a = 4.19 \times 10^5$ kJ/kmole, $K_a = 3.84 \times 10^3$ m^2/s, and $Q_a = 3.352 \times 10^{10}$ J/m^3.

The curves in Fig. 2 show the agglomerate-temperature variation as a function of the agglomerate diameter on the burning surface for various pressures. Ignition and lift-off coincide with the moment of unlimited increase in temperature. The critical value δ_{agl} at which breakdown of thermal equilibrium and unlimited increase in temperature occur corresponds to the finite size of the agglomerate at the moment of ignition and liftoff from the burning surface. With increasing pressure the dependences $T_a(\delta_a)$ in Fig. 2 become closer (curves 3, 4, and 5), and the function $\delta_{\mathrm{agl}}(P)$ with increasing pressure has a certain nonzero limiting value δ^*_{agl}. The mechanism of pressure influence is explained as follows. The stand-off distance H of the kinetic microflame from the solid surface decreases with increasing pressure in accordance with Eqs. (9) and (10), which restricts the degree of agglomerate enlargement and creates conditions

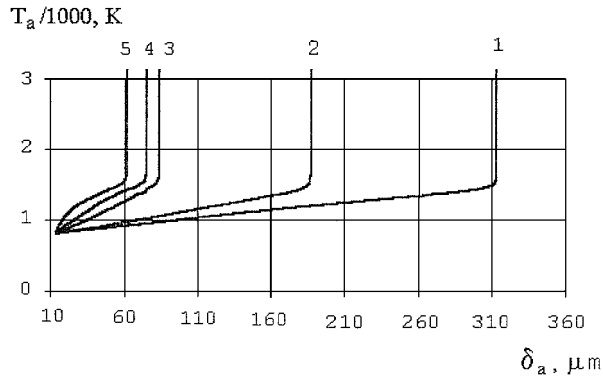

Fig. 2 Temperature of the agglomerate T_a versus its diameter δ_a for different pressures P(MPa): 1—0.04 MPa, 2—0.1 MPa, 3—1.0 MPa, 4—2.0 MPa, 5—4.0 MPa ($\omega_T = 0.9$ mm/s, $D_{ox} = 200$ μm, and $\delta_s = 14$ μm).

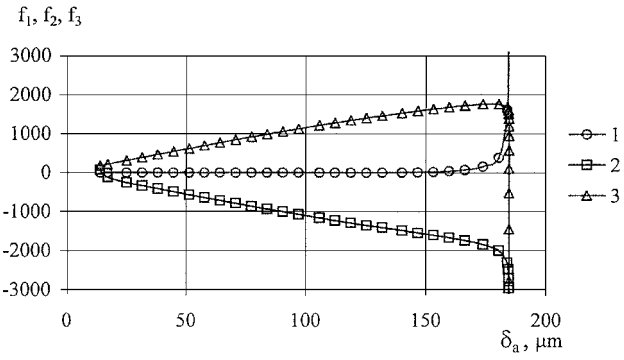

Fig. 3 Change of dimensionless components thermal balance of the agglomerate with the growth of its diameter: 1—oxidizing of aluminum $f_1 = \Omega\Lambda[x/(1 + Z)] \exp[\Theta/(1 + \Delta\Theta)]$; 2—heat exchange by gas and initial particles $f_2 = \Sigma\Theta_g - (3/x + \Sigma)\Theta$; and 3—radiation from the gas phase $f_3 = Ex[(1 + \Delta\Theta_\infty)^4 - (1 + \Delta\Theta)^4]$.

for the formation of several agglomerates within one pocket, so-called prepocket mechanism.[5] At low pressures, where H is high, the agglomerate does not have enough time to ignite, its size becomes comparable with the size of the surface S, and the possibility of contact interaction with similar agglomerates located in the neighboring pockets appears. In this case the interpocket mechanism of agglomeration described in Ref. 5 is operational.

Figure 3 shows the changes in heat-balance components of the agglomerate with increasing diameter of the latter. The influence of the process of aluminum oxidation remains negligible up to the moment of agglomerate ignition initiation. The contribution of the radiation component is significant during the entire residence time of the agglomerate on the surface.

The effect of various initial parameters on the degree of agglomeration was numerically studied. As the dependence of the burning rate on pressure $\omega_T(P)$ used in Eqs. (1–8) becomes stronger, the residence time of particles on the surface and the agglomerate sizes become smaller. With increasing pressure the degree of agglomeration decreases, and there exists a threshold value in terms of pressure, above which $\delta_{agl} = \delta^*_{agl}$ remains constant. It was found[3–6] that the size distribution of AP particles affects the degree of agglomeration so that δ_{agl} varies in proportion to the diameter D_{ox}. The calculated values of $\delta_{agl}(D_{ox})$ are compared with experimental results[3] in Fig. 4. The CSP composition in the calculations corresponded to that in Ref. 3: $\beta_{Al} = 0.12$, $\beta_{ox} = 0.37$, and $\delta_s = 14$ μm. The dependencies of the burning rate on the diameter D_{ox} of AP particles, which were set in the calculations, and the calculated values of agglomerates are listed in Table 1. The agreement between the calculated results and experimental data[3] in Fig. 4 was reached by changing the burning rate shown in Table 1.

D. Generalization of the Model to the Case of a Polydisperse Oxidizer

An important factor that has a significant effect on agglomerate dimensions is the granulometric composition of the oxidizer.

Table 1 Dependence of the burning rate on the diameter D_{ox} of AP particles, and calculated values of agglomerates

P, MPa	D_{ox}, μm	ω_T, mm/s	δ_{agl}, μm
2.0	50	7.5	68
	80	7.5	80
	140	7.5	106
	200	7.5	180
	280	7.5	205
	350	7.5	240
4.0	50	9.0	47
	80	8.9	58
	140	8.5	81
	200	8.0	104
	280	7.7	140
	350	7.0	192

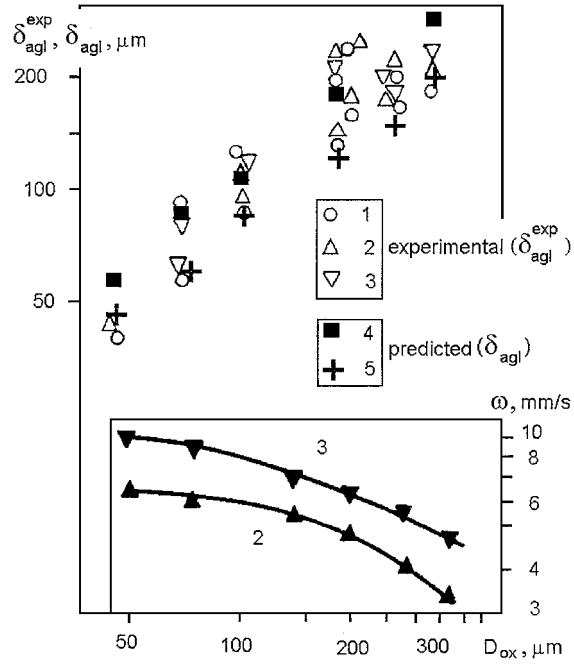

Fig. 4 Effect of the particle diameter of the AP oxidizer D_{ox} on the agglomerate size for the experimental value of the meam-volume diameter δ_{agl} (Ref. 3) (curves 1–3) and the calculated values of δ_{agl} Eq. (39) (curves 4 and 5). P, (MPa): 0.1 (curve 1), 2 (2), 4 (3), 2 (4), and 4 (5).

In studying CSPs with a polydisperse oxidizer, it was found[4,5] that the propellant has a cellular structure formed with participation of AP particles comparable in size. We consider the size distribution function of AP particles and approximate it by a stepwise function with division into N fractions. Within each fraction, we introduce the mean diameter $D_{ox,j}$, such that the following inequalities hold: $D_{ox,1} > D_{ox,2} > \cdots > D_{ox,N}$. Each of N fractions of diameter $D_{ox,j}$ forms a pocket numbered j on the surface, which contains all pockets formed by smaller AP particles (Fig. 5). The CSP cell is assumed to consist of a system of nested pockets. To calculate the area S_j limited by AP particles of diameter $D_{ox,j}$ protruding above the surface, one has to consider a two-phase system "j-particle + pseudobinder," where the pseudobinder consists of binder and aluminum and all smaller AP particles. The number of AP j particles per unit surface is expressed through the volume content

$$N_{ox,j} = \frac{6\beta_{ox,j}}{\pi D^2_{ox,j}}$$

$$\beta_{ox,j} = \frac{\alpha_{ox,j}}{\alpha_{Al}\rho_{ox}/\rho_{Al} + \alpha_f \rho_{ox}/\rho_f + \sum_{k=1}^{j} \alpha_{ox,k}}$$

where $\alpha_{ox,j}$ is the mass fraction of AP j particles. If the number of j particles is rather large and the number of elementary surface of j particles and pseudobinder is roughly identical within a certain

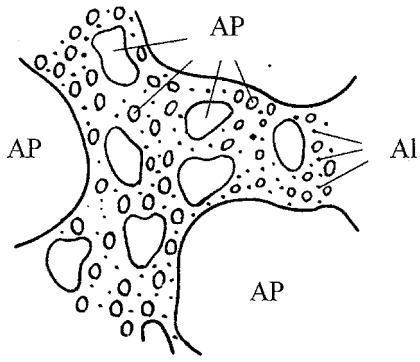

Fig. 5 Surface of the solid propellant containing three AP fractions in the binder matrix with small aluminum particles.

sector on the surface, then the relation $S_j = \pi D_{\text{ox},j}^2(1-\beta_{\text{ox},j})/6\beta_{\text{ox},j}$ is valid under the condition $D_{\text{ox},1} \gg D_{\text{ox},2} \gg \cdots \gg D_{\text{ox},N}$. Part of the area S_j free from AP, from which the initial aluminum particles are united, is

$$S_j^0 = S_j \prod_{k=j+1}^{N} \left(1 - \frac{3\beta_{\text{ox},k}}{2}\right)$$

This allows us to extend Eqs. (1–8) to the case of a polydisperse oxidizer:

$$\frac{d\delta_{a,j}}{dt} = \frac{1}{2}\beta_{\text{Al}}\omega_T \left(1 + \frac{\delta_s}{\delta_{a,j}}\right)^2 \prod_{k=j}^{N-1} \left(1 - \frac{3\beta_{\text{ox},k}}{2}\right) \tag{11}$$

$$\frac{1}{6}\rho_{\text{Al}}\delta_{a,j}^3 c_{\text{Al}} \frac{dT_{a,j}}{dt} = \frac{1}{2}\rho_{\text{Al}}\delta_{a,j}^2 c_{\text{Al}}(T_s - T_{a,j})\frac{d\delta_{a,j}}{dt} + \delta_{a,j}^2\left(q_j + Q_a \frac{d\eta_{a,j}}{dt}\right) \tag{12}$$

$$q_j = \frac{\lambda_g Nu(\tilde{T}_{g,j} - T_{a,j})}{\delta_{a,j}} + \varepsilon_0\sigma_0\left(T_{\infty,j}^4 - T_{a,j}^4\right)$$

$$\frac{d\eta_{a,j}}{dt} = \frac{K_a}{\eta_{a,j}} \exp\left(-\frac{E_a}{R^0 T_{a,j}}\right) \tag{13}$$

The initial conditions for Eqs. (11–13) have the form

$$j = N, \qquad t = 0: \quad T_{a,N} = T_s, \qquad \eta_{a,N} = \eta_s, \qquad \delta_{a,N} = \delta_s \tag{14}$$

Agglomeration of initial aluminum particles starts from pockets of minimum size ($j = N$). If only one agglomerate of diameter $\delta_{a,j}$ comparable with the size of the j pocket remains on the surface S_j, the probability of its contact and merging with identical agglomerates from the neighboring pockets increases. As a result, the transition to a larger $j-1$ pocket occurs, and the interpocket mechanism of agglomeration works. Only paired interactions are considered, where the number of particle agglomerates decreases by a factor of two. On passing to a larger pocket, Eqs. (11–13) are solved again with new initial conditions

$$1 \le j < N, \qquad t = t_j: \quad T_{a,j-1} = T_{a,j}, \qquad \eta_{a,j-1} = \eta_{a,j}, \qquad \delta_{a,j-1} = \delta_{a,j} \tag{14*}$$

where t_j is the transition time. Upon ignition, where the confining relation with the surface is broken, the agglomerate is torn off from the surface and entrained by the ambient gaseous products of decomposition. Aluminum agglomerates can exist without ignition for a long time,[5] which creates conditions for the appearance of superlarge agglomerates. Investigation of ignition of aluminum agglomerates requires a detailed study of the mechanism of formation of local microflames.[4] In combustion of CSP compositions with monodisperse AP, the surfaces of the stoichiometric ratio of the components always close down above AP particles.[30] In the case of polydisperse AP, there is no unambiguous answer to this question. To describe the structure of the combustion wave of a polydisperse AP composite system, Kovalev[35] offered an approximate method based on the idea of nesting of pockets of different size. Each AP particle of radius $a_j = D_{\text{ox},j}/2$ is surrounded by an interlayer of the pseudobinder of radius $b_j > a_j$ containing all AP particles of smaller dimensions and aluminum particles. If we assume that the presence of aluminum particles and their agglomerates on the surface has no significant effect on the surface processes and formation of microflames, then the combustion in the gas phase within each j pocket is described by the system of equations of heat conduction and diffusion of the components[35]:

$$c_p m_T \frac{\partial T_{g,j}}{\partial z_j} - \lambda_g \nabla^2 T_{g,j} = Q_g \Psi, \qquad z_j \ge 0, \qquad 0 \le x_j \le b_j \tag{15}$$

$$m_T \frac{\partial Y_{1,j}}{\partial z_j} - \rho_g \kappa_g \nabla^2 Y_{1,j} = -\chi_1 \nu_1 \Psi \tag{16}$$

$$m_T \frac{\partial Y_{2,j}}{\partial z_j} - \rho_g \kappa_g \nabla^2 Y_{2,j} = -\chi_2 \nu_2 \Psi \tag{17}$$

$$\Psi = K_g \left(\frac{Y_{1,j}P}{R^0 T_{g,j}}\right)^{\nu_1} \left(\frac{Y_{2,j}P}{R^0 T_{g,j}}\right)^{\nu_2} \exp\left(\frac{-E_g}{R^0 T_{g,j}}\right)$$

$$x_j = 0, \qquad x_j = b_j: \quad \frac{\partial Y_{1,j}}{\partial x_j} = \frac{\partial Y_{2,j}}{\partial x_j} = \frac{\partial T_{g,j}}{\partial x_j} = 0 \tag{18}$$

$$z_j = 0: \quad T_{g,j} = T_s$$

$$m_T Y_{(1,2)j} - \rho_g \kappa_g \frac{\partial Y_{(1,2)j}}{\partial z_j} = \begin{cases} m_T, 0, & x_j \le a_j \\ m_T Y^*_{(1,2)j}, & a_j < x \le b_j \end{cases} \tag{19}$$

Equations (15–19) are considered within each j pocket in the cylindrical coordinate system (x_j, z_j), where the axial coordinate z_j changes along the normal to the surface. As a result, the equations of the generalized model (11–19) are localized within the j pocket so that all of the smaller pockets together with AP particles forming them are considered to be averaged over the surface area of this j pocket. This approach allows one to determine the pocket-localized distributions of temperature and concentration of the components. Equations (15–17) yield a linear equation for the function $\beta'_j = Y_{1,j} - \nu Y_{2,j}$, $(\nu = \chi_1\nu_1/\chi_2\nu_2)$, whose solution is expressed through the Bessel functions of the first kind J_0, J_1:

$$\beta'_j(x_j, z_j) = e_j^2 + (1-e_j)^2\left[Y^*_{1,j}(1+\nu) - \nu\right] + 4e_j(1+\nu)\left(1 - Y^*_{1,j}\right)\sum_{k=1}^{\infty} \frac{J_1(\varphi_k e_j)J_0(\varphi_k x_j/b_j)}{\varphi_k J_0^2(\varphi_k)\left[1 + \sqrt{1+(2\psi\varphi_k)^2}\right]} \times \exp\left[-z_j \frac{\sqrt{1+(2\psi\varphi_k)^2} - 1}{2\psi b_j}\right] \tag{20}$$

Here φ_k are the roots of the equation $J_1(\varphi_k) = 0$, $e_j = a_j/b_j$, $\psi = \rho_g\kappa_g/m_T b_j$. It is known[30] that the concentrations of the components on the surface $\beta'_j(x_j, z_j) = 0$ are in a stoichiometric relationship and are not necessarily equal to zero. They might turn to zero at a certain distance from the surface determined by the kinetics of chemical reactions and pressure. The criterion of vanishing of concentrations and formation of a diffuse microflame is the condition of intersection of the stoichiometric surface $\beta'_j(x_j, z_j) = 0$ and

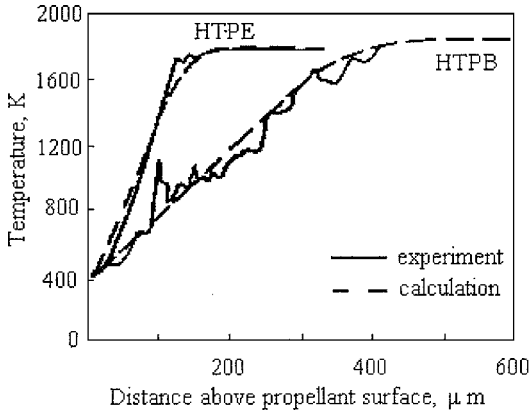

Fig. 6 Temperature profiles in the gas phase ($P = 0.04$ MPa). The —— and – – –, curves refer to the experiment[36] and calculation by Eq. (9).

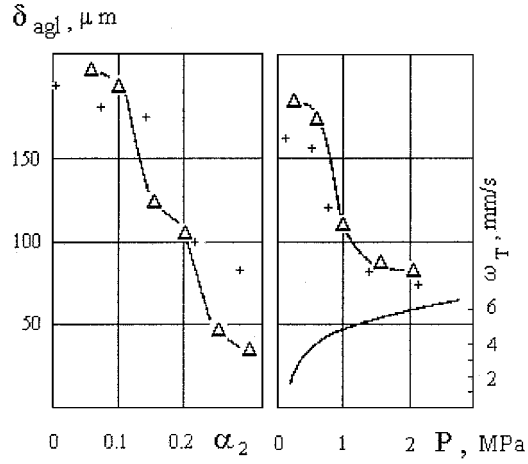

Fig. 7 Dependence of δ_{agl} on the content of the fine AP fraction and pressure: △; calculation and +; experiment[4].

the kinetic microflame.[4] It is obvious that the diffuse microflame is not formed if there is no stoichiometric surface or the kinetic microflame is formed higher than the tip of the stoichiometric surface. The distance at which the kinetic microflame is formed above each individual pocket is determined by solving Eqs. (15–19).

The combustion-wave structure of the AP-based CSP was experimentally studied by methods of thermal analysis.[36] Two types of the binder were used: polybutadiene (HTPB) and polyether with hydroxyl groups (HTPB). The propellant contained 16% of the binder and 84% of bidisperse AP with coarse (200 μm) and fine (20 μm) fractions. The solid lines in Fig. 6 show the typical oscillograms of the temperature distribution in the combustion wave, which were obtained in Refs. 36. Kubota et al.[36] explain the presence of small peaks by a certain number of elementary trickles generated by diffuse microflames. The distance at which the temperature reaches its maximum value is 150 μm for HTPE and 400 μm for HTPB. The oscillograms of temperature distribution in the combustion wave (solid curves) in Fig. 6 are readily approximated by one-dimensional temperature profiles (dashed curves) obtained from Eq. (9). Because heterogeneous combustion of CSPs has not been adequately studied yet, the chemical reaction constants in the gas phase are practically absent in the literature. The following data were used in test calculations[37]: $E_g = 150$ kJ/mole, $Q_g = 2.61 \times 10^6$ J/kg, and $K_g = 6.3 \times 10^{11}$ m^3/(mole · s), which were varied afterwards. The agreement of numerical and experimental data in Fig. 6 is reached by varying the kinetic constants. In particular, the present results were obtained for $K_g = 3.1 \times 10^{13} - 6.5 \times 10^{13}$ m^3/(mole · s), $Q_g = 1.0268 \times 10^7$ J/kg, and $E_g = 150$ kJ/mole.

Figure 7 shows a comparison of theoretical calculations with the experimental data of Ref. 4, where the effect of pressure and content of fine and coarse AP fractions was studied. With decreasing pressure the residence time of particles on the surface increases, which favors the growth of the number of mergence acts, enlargement of agglomerates, and operation of the interpocket mechanism of agglomeration. For a CSP containing large and small AP particles, δ_{agl} drastically decreases at a certain threshold pressure. As the threshold pressure is reached (approximately 0.8–1.0 MPa in Fig. 7), a diffuse microflame is formed on the fine AP fraction located closer to the solid surface of the propellant, which accelerates ignition and entrainment of smaller agglomerates. The mechanism of influence of the content α_2 of the fine AP fraction on δ_{agl} is similar. The diffuse microflame above the fine fraction is not formed until its content becomes noticeable (this is $\alpha_2 = 0.1$–0.2 in Fig. 7).

E. Discussion of Results of Agglomeration Modeling

The just-described physical model of aluminum agglomeration is based on the governing role of aluminum ignition in residence, enlargement, and separation of agglomerates from the burning surface. This assumption is based on filming of burning specimens of the solid propellant,[3–6] where already melted agglomerates of spherical shape leaving the surface at the moment of ignition were usually observed. Based on the notion of a cellular (pocket) structure of the solid propellant, a mathematical model of aluminum agglomeration on the burning surface is proposed. The model allows one to calculate the characteristic diameter of agglomerates with regard for pressure, burning rate, and composition of the solid propellant.

An approximate method is developed for calculation of the combustion-wave structure of the solid propellant with a polydisperse AP oxidizer. Using this method, it is possible to describe the laws of formation of diffuse microflames and their effect on aluminum agglomeration. The granulometric composition of the oxidizer affects the microflame temperature. The lower the microflame temperature, the longer the aluminum agglomerates remain on the surface and are enlarged. The granulometric composition of the AP oxidizer and pressure can exert a significant effect on the agglomerate sizes. The distribution function of AP particle being varied, the stoichiometric surfaces are formed on large and medium-sized particles, when their content becomes greater than 30–35%. The size of agglomerates leaving the surface depends not only on the geometric characteristics of the pocket but are also limited by the thermal boundary-layer thickness, where the gas temperature changes from the surface temperature to the flame temperature. The integral characteristics of the process and the degree of agglomeration are limited by the thermal action of local gas-phase flames, which favor more rapid heating and ignition of agglomerates. Such a mechanism of agglomeration is typical of CSPs that have a "dry" burning surface, that is, liquid-viscous[8,9] or skeleton[5] layers are not formed on the surface. A rather interesting feature of the influence of pressure is observed, whose role is manifested in Eqs. (5–7) through the expression for the chemical reaction rate [Eq. (8)] and the prescribed dependence of the burning rate on pressure $\omega_T(P)$. An increase in pressure leads, on the one hand, to a decrease in the boundary-layer thickness and, on the other hand, to its displacement caused by the increase in the burning rate and injection of decomposition products from the propellant surface. Therefore, the dependence of the burning rate on pressure $\omega_T(P)$, which reflects the features of CSP combustion, can be used to control the size of agglomerates formed.

The agglomeration mechanisms observed (prepocket, pocket, and interpocket[5] mechanisms) are theoretically justified, and the conditions for their existence are determined.

Nevertheless, the proposed physical model of formation of diffuse microflames and the method for calculation of the combustion-wave structure are approximate, pocket-localized, and do not take into account the effect of large pockets on small ones. The lower the ambient pressure and the greater difference in AP fractions (The condition $D_{ox,1} \gg D_{ox,2} \gg \cdots \gg D_{ox,N}$ is satisfied.), the lower this influence. In addition to refinement of the constants of kinetics of chemical reactions in the gas, it is necessary to take into account the changes in the surface temperature T_s with increasing pressure. The initial value of the oxide-film thickness η_s with increasing pressure

should be also refined, because the thickness of the oxide film on initial aluminum particles depends on the velocity of the particles passing through the heated thermal layer.

III. Prediction of Al_2O_3 Particle Sizes in SRM Nozzle

Let us consider a two-phase flow with droplets of identical sizes, in which the concentration of droplets is small, which allows one to neglect their interaction at collisions with each other[15]:

$$\frac{dw_a}{dx} = \varphi_1\left(\frac{w_g}{w_a} - 1\right) \tag{21}$$

$$\frac{dT_a}{dx} = \varphi_2\left(\frac{T_g - T_a}{w_a}\right) \tag{22}$$

$$\rho_g w_g \frac{dw_g}{dx} + \rho_g w_g W \frac{dw_a}{dx} + \frac{dP}{dx} = 0 \tag{23}$$

$$c_p T_a + \frac{w_g^2}{2} + W\left(c_b T_a + \frac{w_a^2}{2}\right) = E_0 \tag{24}$$

$$\rho_g w_g F = m_0 \tag{25}$$

$$P = \rho_g \frac{R^0}{\chi_g} T_g \tag{26}$$

Here E_0 and m_0 are constants. The particle/gas fraction W for a steady flow is assumed to be constant. The flow cross-sectional area F is defined by the nozzle contour $F = \pi R^2(x)$. The relaxation times of the velocity and temperature lag of particles relative to the gas φ_1^{-1}, φ_2^{-1} have the form

$$\varphi_1 = \frac{18\mu_g}{\delta^2 \rho_b}, \qquad \varphi_2 = \frac{6Nuc_p\mu_g}{Pr\rho_b c_b \delta^2} \tag{27}$$

To take into account the features of aerodynamic splitting of particles, we consider the Weber criterion in addition to Eqs. (21–27):

$$We = \frac{\rho_g(w_g - w_a)}{\sigma_b} \le We_t \tag{28}$$

As the Weber number We in a certain cross section of the nozzle reaches the critical value We_t, all particles are split simultaneously to an identical number of fragments equal in mass in this cross section. This rigorous restriction, at first sight, leaves us within the framework of the flow model (21–27) and, as we will see later, does not restrict the generality of the result.

A. Approximate Analytical Solution

If the lag of particles from the gas is small, Eqs. (21–27) can be linearized in terms of a small parameter that characterizes the degree of this lag. In particular, according to Kovalev and Fomin,[29] we have

$$w_g - w_a \cong \frac{w_e}{\varphi_1}\frac{dw_e}{dx} \tag{29}$$

The parameters of the equilibrium flow in the nozzle are determined by the formulas

$$\rho_e = (1 + W)\rho_g, \qquad c_p^e = \frac{c_p + c_b W}{1 + W}, \qquad c_v^e = \frac{c_v + c_b W}{1 + W}$$

$$k_e = \frac{c_p^e}{c_v^e}, \qquad R_e^0 = c_p^e - c_v^e \tag{30}$$

$$w_e = a_e^* \gamma_e \left(\frac{2}{k_e + 1}\right)^{\frac{1}{2}} \tag{31}$$

$$P_e = P_e^*\left(1 - \frac{k_e - 1}{k_e + 1}\gamma_e^2\right)^{k_e/(k_e - 1)} \tag{32}$$

$$\rho_e = \rho_e^*\left(1 - \frac{k_e - 1}{k_e + 1}\gamma_e^2\right)^{1/(k_e - 1)} \tag{33}$$

$$\frac{F}{F_t} = \frac{1}{\gamma_e}\left[\frac{2/(k_e + 1)}{1 - \gamma_e^2(k_e - 1)/(k_e + 1)}\right]^{1/(k_e - 1)} \tag{34}$$

Here $a_e^* = \sqrt{(k_e P_e^*/\rho_e^*)}$, P_e^*, ρ_e^* are the velocity of sound, pressure, and density in the frozen equilibrium flow.

From Eq. (28), taking into account Eqs. (27), (29), and (32), we can easily evaluate the admissible particle size as a function of x:

$$\delta(x) = \left\{\frac{We_t(18\mu_g)^2\sigma_b(1 + W)}{\rho_b^2 \rho_e (w_e dw_e/dx)^2}\right\}^{\frac{1}{5}} \tag{35}$$

Each cross section of the nozzle will not allow droplets larger than $\delta(x)$ to pass without shattering. Assuming that $dR/dx = \xi$, in the case of finite curvature of the contour, we can readily show that the function $\delta(\gamma_e)$ will reach a minimum at the throat F_t. Obviously, the derivative dw_e/dx is undetermined for $\xi = 0$ and $\gamma_e = 1$. We represent it in the form

$$\frac{dw_e}{dx} = \frac{f_1(\gamma_e, x)}{f_2(\gamma_e, x)} \tag{36}$$

$$f_1(\gamma_e, x) = 2a_e^* R(x)\xi(x)\left(\frac{2}{k_e + 1}\right)^{(k_e - 3)/2(k_e - 1)} \times \gamma_e^2\left(1 - \frac{k_e - 1}{k_e + 1}\gamma_e^2\right)^{k_e/(k_e - 1)}$$

$$f_2(\gamma_e, x) = R_t^2\left(\gamma_e^2 - 1\right)$$

We assume that the following expressions are valid in the nozzle throat:

$$\left.\frac{dw_e}{dx}\right|_{x = x_t} = w'_{et}, \qquad w_e(x) - w_{et} = w'_{et}(x - x_t) \tag{37}$$

Here w_{et} is the equilibrium velocity in the throat. We expand the functions f_1 and f_2 into the Taylor series for $x = x_t$. We obtain an algebraic equation for the derivative w'_{et}, which follows from Eqs. (36) and (37) and depends on (with regard for the curvature radius of the nozzle throat R_C)

$$\left.\frac{dw_e}{dx}\right|_{x = x_t} = \frac{2\sqrt{2}a_e^*}{(k_e + 1)\sqrt{R_C D_t}}, \qquad \frac{1}{R_C} = \frac{d^2R}{dx^2} \tag{38}$$

where $D_t = 2R_t$ is the nozzle-throat diameter. The particle/gas fraction W is easily calculated from the mass fraction α_{Al} of aluminum in the propellant if the two-phase flow is assumed to be steady. The flow rate of particles $\rho_a w_a$ (where ρ_a is the mean density of particles) and the flow rate of the gas $\rho_g w_g$ per unit area depend on the mean burning rate ω_T and propellant density ρ_T and are constants: $\rho_a w_a = \alpha_{Al}\rho_T\omega_T$, $\rho_g w_g = (1 - \alpha_{Al})\rho_T\omega_T$. It follows from here that $W = \rho_a w_a/(\rho_g w_g) = \alpha_{Al}/(1 - \alpha_{Al})$. This ratio is an approximate estimation obtained from the following assumptions. Burning of aluminum particles in products of solid propellant is a very complicated process. Certainly at aluminum burning the properties of both the own particle (turns into aluminum oxide) and gas containing the vapors of aluminum and its compounds change. So consumptions of gas and particles will not be constant. However, one can assume that at a stationary flow a ratio of these consumptions in one and the same section of the nozzle is either constant or negligibly little change.

Table 2 Comparison of the particle size δ_t calculated by Eq. (39) and the Al_2O_3 particle size data summary, Ref. 27

Item no.	Motor	Propellant	% Al	ξ_C	T_C, ^OR	$\bar{P}_C$, psia	D_t, in.	R_C/R_t	$\bar{\tau}$, ms	$D_{43}^{\exp}$, μm	D_{43}^{cor}, μm	δ_t, μm
1	156-5	LPC-58OA 87% solids PBAN	18	0.32	6260	667	60.4	0.5	113	**10.9**	**12.08**	**11.37**
2	156-6	LPC-58OC 87% solids PBAN	18	0.32	6260	664	34.5	0.6	110	**11.1**	**10.25**	**9.44**
3	156-7	TP-H8163 86% solids PBAN	16	0.26	6110	560	20.0	3.0/1.0	143	**10.8**	**8.73**	**10.78**
4	156-9	TP-H1115 87% solids PBAN	18	0.32	6400	560	34.5	0.9/0.8	110	**12.0**	**10.25**	**10.54**
5	TCC-120	TP-H1085 88.5% solids CTPB	20	0.34	6260	700	24.5	0.9/0.5	162	**11.1**	**9.27**	**8.92**
6	TCC-120	TP-H1077 86% solids PBAN	16	0.26	6110	——	21.3	——	——	**8.6**	——	——
7	UA-1205	UTR-3001 84% solids PBAN	16	0.285	5960	550	37.7	0.4	175	**12.0**	**10.52**	**9.36**
8	260-SL2	ANB-3105 85% solids PBAN	15	0.26	5990	489	71.0	1.0	202	**12.9**	**12.66**	**14.74**
9	260-SL3	ANB-3254 85% solid PBAN	15	0.26	5990	559	89.1	0.7	143	**13.3**	**13.54**	**14.64**
10	44SS4	ANB-3254 85% solids PBAN	15	0.26	5990	495	15.5	0.75/1.0	23	**8.89**	**7.38**	**7.55**
11	Poseidon/FS	TP-H1114 86% solids PBAN	16	0.26	6170	870	11.6	1	116	**8.75/6.2**	**7.44**	**6.36**
12	MM/S wing II	ANP-2864 82% solids PU	17	0.293	6090	460	8.5	3	60.3	**5.8**	**6.79**	**8.00**
13	Super BATES	UTP-18, 803A 90% solids HTPB	21	0.357	6670	1000	8.0	2	74	**5.23**	**6.67**	**6.18**
14	MM/FS 65-in.	TP-H1011 86% solids PBAN	16	0.26	6120	650	7.5	1	91	**8.98**	**6.55**	**5.67**
15	45 in.	UTP-15, 908 90% solids HTPB 25% HMX	18	0.305	6320	950	4.14	4	145	**6.23**	**5.50**	**5.50**
16	C4/TS ADP	UTP-15, 908 90% solids HTPB 25% HMX	18	0.305	6320	1000	4.04	4	90	**6.17**	**5.46**	**5.37**
17	MX/S ADP	PEG/FEFO 84% solids	18	0.297	6770	1250	6.91	2/1	157	**5.77**	**6.39**	**5.47**
19	Shuttle staging motor	UTP-19, 048 86% solids HTPB	2	0.036	5390	1700	3.2	1.5	6.5	**1.14**	**1.41**	**3.77**
20	CSD-TM-3	UTP-15, 151 90% solids HTPB 25% HMX	18	0.310	6280	770	2.3	2	54	**5.33**	**4.63**	**3.94**
21	CSD-TM-3	UTP-15, 151 90% solids HTPB 25% HMX	18	0.305	6320	1093	2.04	2	69	**4.38**	**4.47**	**3.50**
22	CSD-TM-3	UTP-15, 908 90% solids HTPB 25% HMX	18	0.305	6320	980	2.03	2	69	**5.36**	**4.46**	**3.57**
23	70-1b BATES	RH-P-112 45% solids CMDB	20	0.271	6140	1200	2.1	2	16	**2.63**	**4.44**	**3.53**
24	70-1b BATES	RH-P-112 45% solids CMDB	20	0.271	5960	400	3.73	2	5.2	**5.41**	**1.96**	**5.56**
25	70-1b BATES	ANP-2969 75% solids PU	20	0.34	6440	1000	1.48	2	35	**2.34**	**4.07**	**3.15**
26	70-1b BATES	ANP-3066 88% solids CTPB	15	0.25	6290	1000	1.76	2	27	**1.93**	**4.26**	**3.31**
27	70-1b BATES	TP-H-1120 86% solids PBAN	16	0.26	6125	500	3.21	2	6.9	**2.72**	**2.65**	**4.88**
28	70-1b BATES	TP-H-8163 86% solids PBAN	16	0.26	6240	1000	2.00	2	18	**2.11**	**4.35**	**3.50**
29	70-1b BATES	TP-H-8163 86% solids PBAN	16	0.26	6110	550	2.46	2	12	**2.00**	**3.56**	**4.31**
30	70-1b BATES	LPC-580A 87% solids PBAN	18	0.32	6330	1000	2.52	2	13	**2.66**	**4.60**	**3.87**
31	9C7.5-17.1	RH-P-178 56% solids CMDB	21	0.36	6670	1000	1.70	2	17	**2.60**	**4.21**	**3.32**
32	9C7.5-17.1	RH-SE-108 63% solids TVOPA	15	0.25	6380	1000	1.70	2	16	**1.90**	**4.07**	**3.25**
33	10KS-2500	82% solids polyurethane	17	0.292	6010	1000	1.9	2	32	**4.59**	**4.37**	**3.48**
34	3KS-1000	82% solids polyurethane	17	0.292	6010	1000	0.9	2	15	**4.41**	**3.42**	**2.58**
35	3KS-1000	82% solids polyurethane	17	0.31	5580	200	1.6	2	5	**1.2**	**0.93**	**4.55**
36	3KS-1000	82% solids polyurethane	15	0.258	5900	1000	0.9	2	15	**4.35**	**3.37**	**2.56**

(Continued)

Table 2 Comparison of the particle size δ_t calculated by Eq. (39) and the Al_2O_3 particle size data summary, Ref. 27(continued)

Item no.	Motor	Propellant	% Al	ξ_C	T_C, ^OR	$\bar{P}_C$, psia	D_t, in.	R_C/R_t	$\bar{\tau}$, ms	D_{43}^{exp}, μm	D_{43}^{cor}, μm	δ_t, μm
37	3KS-1000	82% solids polyurethane	19	0.326	6140	1000	0.9	2	15	**4.48**	**3.45**	**2.59**
38	3KS-1000	82% solids polyurethane	3	0.052	5220	1000	0.9	2	12	**3.11**	**1.40**	**2.48**
39	1KS-250	82% solids polyurethane	17	0.292	6010	1000	0.3	2	6	**0.75**	**1.94**	**1.66**
40	1KS-250	82% solids polyurethane	3	0.052	5220	1000	0.3	2	5	**0.25**	**0.48**	**1.83**
41	HI-5PC	DDP-08 41% solids CMDB	20.9	0.368	7020	1000	0.8	2	6.5	**3.12**	**2.91**	**2.43**
42	HI-5PC	DDP-08 41% solids CMDB	20.9	0.368	6980	800	0.95	2	4.6	**3.23**	**2.39**	**2.73**
43	HI-5PC	DDP-08 41% solids CMDB	20.9	0.368	6920	600	1.1	2	3.4	**3.21**	**1.71**	**3.07**
44	3KS-500	ANB-3254 85% solids PBAN	15	0.26	6060	1000	1.0	0.5	3.9	**2.15**	**2.04**	**2.01**
45	15-1b BATES	RH-P-112 45% solids CMDB	20	0.271	6100	1000	1.28	2	8.3	**2.19**	**3.00**	**3.00**
46	CSD-TM-1	UTP-15,908 90% solids HTPB 25% HMX	18	0.305	6340	1116	0.70	2	25	**4.99**	**3.26**	**2.27**
47	CSD-TM-1	UTP-15,908 90% solids HTPB 25% HMX	18	0.305	6350	1368	0.65	2	29	**4.76**	**3.19**	**2.11**
48	CSD-TM-1	UTP-15,945 88% solids HTPB	18	0.315	6320	885	1.31	2	7.1	**2.61**	**3.14**	**3.05**
49	CDS-4 1b	UTP-11,475 88% solids CTPB	18	0.299	6470	1000	0.625	2	11.7	**3.00**	**2.98**	**2.21**
50	CSD-4 1b	UTP-13,945 88% solids HTPB	18	0.315	6340	997	0.835	2	6.8	**3.56**	**2.84**	**2.49**
51	CSD-4 1b	UTP-15,158 90% solids CTPB 34% HMX	16.5	0.28	6130	1000	0.578	2	13.7	**2.46**	**2.95**	**2.14**
52	CSD-4 1b	UTP-15,908 88% solids HTPB 25% HMX	18	0.305	6320	1030	0.544	2	15.8	**3.06**	**2.98**	**2.08**
53	CSD-3C2-X	UTP-3096 84% solids PBAN	16	0.277	6030	1100	0.25	2	67	**4.09**	**2.41**	**1.51**
54	CSD-3C2-X	UTP-3096 84% solids PBAN	16	0.277	6060	1000	0.50	2	67	**4.08**	**2.96**	**2.03**
55	CSD-3C2-X	UTP-3096 84% solids PBAN	16	0.277	5960	630	0.50	2	68	**3.64**	**2.96**	**2.23**
56	CSD-3C2-X	UTP-3096 84% solids PBAN	16	0.270	5640	115	0.50	2	71	**0.52**	**2.47**	**3.17**
57	CSD-3C2-X	UTP-3096 84% solids PBAN	16	0.277	6030	970	0.50	2	33	**3.23**	**2.94**	**2.04**
58	CSD-3C2-X	UTP-3096 84% solids PBAN	16	0.277	5980	730	0.50	2	33	**2.54**	**2.94**	**2.16**
59	CSD-3C2-X	UTP-3096 84% solids PBAN	16	0.273	5680	140	0.50	2	35	**1.04**	**1.96**	**3.04**
60	CSD-3C2-X	UTP-3096 84% solids PBAN	16	0.277	6030	980	0.50	2	14	**2.99**	**2.82**	**2.03**
61	CSD-3C2-X	UTP-3096 84% solids PBAN	16	0.277	5970	650	0.50	2	15	**2.69**	**2.63**	**2.21**
62	CSD-3C2-X	UTP-3096 84% solids PBAN	16	0.276	5930	470	0.50	2	15	**2.20**	**2.35**	**2.36**
63	CSD-3C2-X	UTP-3096 84% solids PBAN	16	0.27	5640	110	0.50	2	17	**0.93**	**1.00**	**3.19**
64	CSD-3C2-X	UTP-3096 84% solids PBAN	16	0.274	5760	190	1.00	2	8	**1.05**	**1.04**	**3.76**
65	CSD-3C2-X	UTP-4574 82% solids PBAN	5	0.091	5260	600	0.50	2	15	**1.05**	**1.44**	**2.19**
66	2C1.5-4	UTP-13,945 88% solids HTPB	18	0.315	6340	997	0.335	2	4.1	**2.46**	**1.71**	**1.73**

Then an approximate value $W = \alpha_{Al}/(1-\alpha_{Al})$ is true. Substituting Eq. (38) into Eq. (35), we obtain

$$\delta_t = \left[162 R_C D_t \left(1 + \frac{\alpha_{Al}}{1-\alpha_{Al}}\right) \frac{\sigma_b We_t}{\rho_b^2} \times \frac{\mu_g^2}{k_e^2 R_e^0 T_e^* P_e^*} \left(\frac{k_e+1}{2}\right)^{(3k_e-2)/(k_e-1)} \right]^{\frac{1}{5}} \tag{39}$$

Because the stagnation parameters of the equilibrium flow are approximately equal to the corresponding parameters in the combustor $P_e^* \approx P_C$, $T_e^* \approx T_C$, and using Eq. (30) to determine k_e, formula (39) allows one to calculate the limiting particle size δ_t at the throat for a given nozzle geometry, pressure, and temperature in the combustor. This size is the lower limit for large particles (Their diameters should tend to this limit as a result of aerodynamic fragmentation.) and the upper limit for small particles. (Their diameters should tend to this limit as a result of coagulation during collisions.)

Kovalev and Fomin's calculations[29] of one-dimensional equations of a polydisperse two-phase flow in the Laval nozzle (with coagulation and the Lagrange and Weber breakup) show that the mean-mass diameter of droplets in the throat and at the nozzle exit coincides rather accurately with δ_t predicted by Eq. (39). Results of multidimensional numerical studies of two-phase polydisperse nozzle flows are known, which were performed at a high level of mathematical and numerical simulation including coagulation and breakup of droplets.[22–24] The mean-mass diameter of particles changes most significantly in the subsonic part of the nozzle. For a moderate volume concentration of particles ($\sim 10^{-5} - 10^{-4}$), which is typical of propellants with a moderate content of aluminum, the mean-mass diameter in the supersonic part of the flow changes weakly along the nozzle, and the difference between its values at the nozzle exit and in the throat is small. This agrees, partly, with Salita's results.[38]

The analysis of calculations[22–24,29] allows us to speak about the possibility of using formula (39) for estimation of the droplet size not only in the throat but also at the nozzle exit.

B. Analysis of Results and Comparison with Experimental Data

The measured values of mean-mass diameter D_{43} in exhaust plumes of a large number of small and medium-sized rocket engines were listed by Hermsen[27] (and are repeated here as Table 2). This table contains the geometric characteristics of the nozzle, compositions of solid propellants, and parameters of its burning in the combustion chamber at which D_{43} was measured. The notation of parameters in Tables 2 and their dimensions correspond to those accepted in Ref. 27: ξ_C is the aluminum-oxide concentration under combustor conditions, g · mole/100 g; T_C is the Rankine temperature in the combustor, ^{O}R; P_C is the pressure in the combustor, psia; R_t or D_t is the radius or diameter of the nozzle throat, in.; R_C is the curvature radius of the nozzle throat, in.; $\bar{\tau}$ is the residence time in the combustor, ms; Re_t is the Reynolds number in the nozzle throat. According to Hermsen, the mean-mass diameter D_{43} of the Al_2O_3 particles in exhaust plumes (data of Table 2) is adequately approximated by the empirical correlation

$$D_{43}^{\text{cor}} = 3.6304 D_t^{0.2932} [1 - \exp(-0.0008163 \xi_C P_C \bar{\tau})] \qquad (40)$$

Formula (40) is recommended in Ref. 27 as the best one and, in Ref. 40 yields good agreement with result of particle-size measurements in the plume of a large-scale engine of the Shuttle class. Figure 8 shows a comparison of the values of δ_t calculated theoretically by formula (39) to the measured data used by Hermsen. Agreement is comparable to that demonstrated by Hermsen's correlation (40) of the data (Fig. 9). In evaluating Eq. (39), the following parameters were specified for liquid drops of Al_2O_3 (according to Ref. 39, p. 246, at the melting point $T_m = 2303$ K): $\rho_b = 3060$ kg/m^3, $\sigma_b = 0.7$ N/m, and $c_b = 1400$ J/(kg K). The values of gas-dynamic parameters were chosen in the form $\mu_g = 6.55 \times 10^{-5}$ N · s/m^2, $c_p = 1922$ J/(kg K), $R_g = R^0/\chi_g = 397$ J/(kg K), and $We_t = 22$.

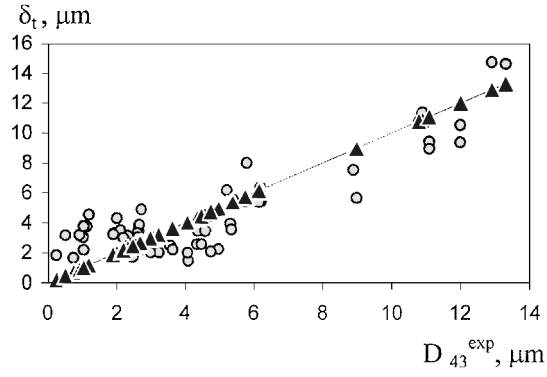

Fig. 8 Comparison of the particle size δ_t (○) calculated by Eq. (39) and the mean-mass diameter D_{43}^{exp} (Ref. 27) (△).

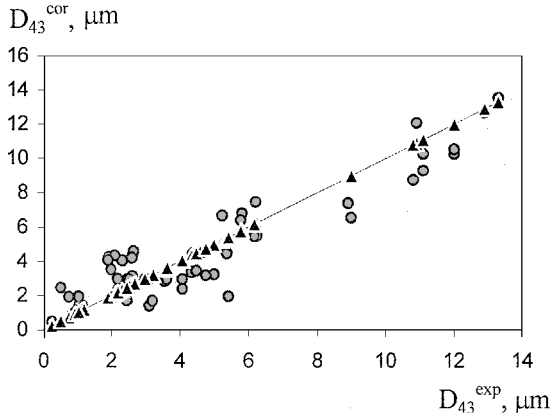

Fig. 9 Comparison of the particle size D_{43}^{cor} (○) calculated by the correlation dependence [Eq. (40)] and the mean-mass diameter D_{43}^{exp} (Ref. 27) (△).

IV. Conclusions

The discrepancies observed in Figs. 8 and 9 are a little different, which allows us to argue that formula (39) can be used to evaluate the mean particles diameter at the nozzle exit. This is also evidenced by the fact that the results of numerical simulation of polydisperse two-phase flows yield a mean-mass particle diameter $D_{43}(x)$ in the nozzle throat, which is barely different from the limiting diameter δ_t and remains almost unchanged until the nozzle exit.[22–24] The disagreement with experimental results can be attributed to the following reasons:

1) Table 2 (Ref. 27) contains no gas parameters (dynamic viscosity μ_g, gas constant R_g, and specific heat capacity at constant pressure c_p) necessary for formula (39); therefore, they were estimated approximately and then remained constant in all calculations.

2) The particle-material properties ρ_b, c_b, σ_b depend on temperature.

3) If the particle concentration in the flow is small (as was the case in experiment Nos. 19, 38, 40, and 65 with aluminum content in the propellant equal to 2, 3, and 5%, respectively, Table 2), then the mean-mass particle diameter has not enough time to reach the limiting value δ_t. Therefore, the difference with these experiment was more than 100%.

4) It is difficult to explain why such low values of D_{43}^{exp} are obtained at low pressures (experiment Nos. 35, 56, 59, and 63, Table 2). On the one hand, the low pressure in the combustor favors the growth of agglomerates of aluminum particles on the burning surface[1–7]; on the other hand, the force action of the gas on the particles at low pressure is rather small, and the degree of particle breakup cannot be that high.

The limits of applicability of formula (39) are directly related to the content of aluminum in the propellant. Obviously, if the concentration of aluminum is low (less than 5–10%), then the mean-mass particle diameter can fail to reach the limiting size, and the error is large. For high contents of aluminum (more than 25%), the particle concentration can be so high that it will exert a choking effect in the two-phase flow[25] with strong competition of the processes of aerodynamic fragmentation and coagulation of particles. As a result, the mean-mass particle diameter will be greater than the admissible limiting value.

Nevertheless, in all other cases, where the content of aluminum is neither very high nor very low, which is a typical situation for advanced solid rocket motors, formula (39) is not worse than Hermsen's correlation (40). In contrast to (40), formula (39) is a physically well-grounded, multiparametric dependence and contains 11 independent physical parameters, which can be readily calculated and prescribed. A comparison of theoretical calculations with the Hermsen's empirical correlation and experimental data of Refs. 27, 28, and 40 allows us to recommend this formula for predicting the size of Al_2O_3 particles in exhaust plumes of a wide class of solid rocket motors.

Acknowledgments

The author is grateful to V. M. Fomin, a corresponding member of the Russian Academy of Sciences, who initiated the first part of this work,[29] and to V. E. Zarko, whose comments significantly improved the present work.

References

[1]Povinelli, L. A., and Rosenstein, R. A., "Alumina Size Distributions from High-Pressure Composite Solid Propellant Combustion," *AIAA Journal*, Vol. 2, No. 10, 1964, pp. 1754–1760.

[2]Gany, A., and Caveny, L. H., "Aluminized Solid Propellants Burning in a Rocket Motor Flowfield," *AIAA Journal*, Vol. 16, No. 7, 1978, pp. 736–739.

[3]Grigoriev, V. G., Zarko, V. E., and Kutsenogii, K. P., "Experimental Study of Aluminum Agglomeration by Combustion of Mixed Compositions," *Combustion, Explosion, and Shock Waves*, Vol. 17, No. 3, 1981, pp. 3–10.

[4]Sambumurthi, J. K., Price, E. W., and Sigman, R. K., "Aluminum Agglomeration in Solid-Propellant Combustion," *AIAA Journal*, Vol. 22, No. 8, 1984, pp. 1132–1138.

[5]Babuk, V. A., Belov, V. P., Khodosov, V. V., and Shelukhin, G. G., "Investigation of the Agglomeration of Aluminum Particles During the Combustion of Metallized Composite Condensed Systems," *Combustion, Explosion, and Shock Waves*, Vol. 21, No. 3, 1985, pp. 287–291.

[6]Duterque, J., "Experimental Studies of Aluminum Agglomeration in Solid Rocket Motors," *4th International Symposium on Special Topics in Chemical Propulsion*, ONERA TP 1996-48, Stockholm, Sweeden, 1996, pp. 1–10.

[7]Glotov, O. G., Zarko, V. E., Karasev, V. V., and Beckstead, M. W., "Condensed Combustion Products of Metalized Propellants of Variable Formulation," AIAA Paper 98-0449, 1998, p. 7.

[8]Gladun,V. D., Frolov, Yu. V., and Kashporov, L. Ya., " The Mechanism of Agglomeration in Combustion of Metalized Condensed Systems," Div. of the Institute of Chemical Physics, Russian Academy of Sciences, Chernogolovka, 1977, pp. 1–41.

[9]Gany, A., and Caveny, L., "Agglomeration and Ignition Mechanism of Aluminum Particles in Solid Propellants," *17th Symposium (International) on Combustion*, Combustion Inst., Pittsburgh, PA, 1979.

[10]Grigoriev, V. G., Koutsenogii, K. P., and Zarko, V. E., "A Model of Aluminum Agglomeration by Combustion of Mixed Compositions," *Combustion, Explosion, and Shock Waves*, Vol. 17, No. 4, 1981, pp. 9–17.

[11]Cohen, N. S., "A Pocket Model for Aluminum Agglomeration in Composite Propellants," *AIAA Journal*, Vol. 21, No. 5, 1983, pp. 720–725.

[12]Kovalev, O. B., "Physico-Mathematical Modelling of Aluminum Agglomeration by Combustion of Mixed Condensed Systems," *Combustion, Explosion, and Shock Waves*, Vol. 25, No. 1, 1989, pp. 39–48.

[13]Lun, S. P., Lin, T. K., and Perng, H. C., "Pocket Model Application to the Combustion of AP/RDX/AL/HTPB Propellants," *31st AIAA/ASME/SEA/ASEE Joint Propulsion Conference and Exhibit*, San Diego, CA, July 1995, pp. 1–6.

[14]Salita, M., "Deficiencies and Requirement in Modeling of Slag Generation in Solid Rocket Motors," *Journal of Propulsion and Power*, Vol. 11, No. 1, 1995, pp. 10–23.

[15]Kliegal, J. R., and Nickerson, G. R., "Flow of Gas-Particle Mixtures in Axially Symmetric Nozzles," *Detonation and Two-Phase Flow*, Academic Press, New York, 1962, pp. 173–194.

[16]Kraiko, A. N., and Sternin A. E., "Theory of the Flow of a Two-Phase Continuous Medium with Solid or Liquid Particles," *Zhurnal Prikladnoi Matematiki i Mekhaniki*, Vol. 29, No. 3, 1965, pp. 418–429.

[17]Crowe, C. T., and Willoughby, P. G., "A Study of Particle Growth in a Rocket Nozzle," *AIAA Journal*, Vol. 5, No. 7, 1967, pp. 1300–1304.

[18]Marble, F. E., "Droplet Agglomeration in Rocket Nozzles Caused by Particle Slip and Collision," *Astronautica Acta*, Vol. 13, No. 2, 1967, pp. 159–166.

[19]Grishin, S. D., Tishin, A. P., and Khairugdinov, R. I., "Nonequilibrium Two-Phase Flow in the Laval Nozzle with Coagulation of Polydisperse Condensate Particles," *Izvestiya AN SSSR, Mekhanika Zhidkosti i Gaza*, No. 2, 1969, pp. 112–117.

[20]Rudinger, G., "Gas-Particle Flow in Convergent Nozzles at High Loading Ratio," *AIAA Journal*, Vol. 8, No. 7, 1970, pp. 1288–1293.

[21]Babukha, G. L., Sternin, L. E., and Shraiber, A. A., "Calculation of Two-Phase Losses in Nozzles with Coagulation and Fragmentation of Condensed Droplets," *Izvestiya AN SSSR, Mekhanika Zhidkosti i Gaza*, No. 1, 1971, pp. 175–177.

[22]Kisarov, Yu. F., and Lipanov, A. M., " Calculation of the Parameters of a Two-Phase Flow in Axisymetric de Laval Nozzle with Regard to the Coagulation and Fragmentation of Particles," *Izvestiya AN SSSR, Mechanika Zhidkosti i Gaza*, No. 4, 1975, pp. 42–46.

[23]Vasenin, I. M., Narimanov, R. K., Glasunov, A. A., Kuvshinov, N. E., and Ivanov, V. A., "Two-Phase Flows in the Nozzles of Solid Rocket Motors," *Journal of Propulsion and Power*, Vol. 11, No. 4, 1995, pp. 583–592.

[24]Bondarchuk, S. S., Vorozhtsov, A. B., Kozlov, E. A., and Feshenko, Y. V., "Analysis of Multidimensional and Two-Phase Flow in Solid Rocket Motors," *Journal of Propulsion and Power*, Vol. 11, No. 4, 1995, pp. 593–599.

[25]Yanenko, N. N., Soloukhin, R. I., Papyrin, A. N., and Fomin, V. M., *Supersonic Two-Phase Flows Under Non-Equilibrium of the Particle Velocities*, Nauka, Novosibirsk, 1980, p. 160.

[26]Nigmatulin, R. I., *Dynamics of Multiphase Media*, Part I, Nauka, Moscow, 1987, pp. 1–464.

[27]Hermsen, R. W., "Aluminum Oxide Particle Size for Solid Rocket Motor Performance Prediction," *Journal Spacecraft and Rockets*, Vol. 18, No. 6, 1981, pp. 483–490.

[28]Laredo, D., McCrorie, J. D. II, Vaghn, J. K., and Netzer, D. W., "Motor and Plume Particle Size Measurements in Solid Propellant Micromotors," *Journal of Propulsion and Power*, Vol. 10, No. 3, 1994, pp. 410–418.

[29]Kovalev, O. B., and Fomin, V. M., "Analytical Investigation of Two-Phase Mixture Flow in a Nozzle with Airdynamical Fractionation Taken into Account," *Combustion, Explosion, and Shock Waves*, Vol. 18, No. 5, 1982, pp. 83–89.

[30]Beckstead, M. W., Derr, R. L., and Price, C. F., "A Model of Composite Solid Propellant Combustion Based on Multiple Flames," *AIAA Journal*, Vol. 8, No. 12, 1970, pp. 2200–2207.

[31]Polishchyuk, D. I., Shevchuk, V. G., Velikanova, V. L., Goroshin, S. V., and Nechitalio, I. N., "Critical Ignition Conditions for Conglomerates of Aluminum Particles," *Combustion, Explosion, and Shock Waves*, Vol. 14, No. 2, 1978, pp. 175–177.

[32]Glick, R. L., "Distribution Functions for Statistical Analysis of Monodispersed Composite Solid Propellant Combustion," *AIAA Journal*, Vol. 14, No. 11, 1976, pp. 1631–1633.

[33]Kovalev, O. B., Petrov, A. P., and Folts, A. V., "On Modelling of Agglomeration Process of Powder Aluminium by Combustion of Condensed Systems," *Combustion, Explosion, and Shock Waves*, Vol. 23, No. 2, 1987, pp. 17–21.

[34]Kovalev, O. B., "Pysico-Mathematical Modeling of Aluminium Agglomeration by Combustion of Mixed Condensed Systems," *Combustion, Explosion, and Shock Waves*, Vol. 25, No. 1, 1989, pp. 39–47.

[35]Kovalev, O. B., "Approximate Structural Calculation of Combustion Wave for Composite Condensed systems," *Flame Structure*, Vol. 1, edited by O. P. Korobeinichev, Inst. of Chemical Kinetics and Combustion SB RAN, Nauka, Novosibirsk, 1991, pp. 254–257.

[36]Kubota, N., Kuwahara, T., Myazaki, S., Uchiyama, K., and Hirata, N., "Combustion Wave Structures of Ammonium Perchlorate Composite Propellants," *Journal of Propulsion and Power*, Vol. 2, No. 4, 1986, pp. 296–300.

[37]Shanon, L. J., and Deverall, L. I., "A Model of Solid-Propellant Ignition in a Neutral Environment," *AIAA Journal*, Vol. 7, No. 3, 1969, pp. 497–502.

[38]Salita, M., "Use of Water and Mercury Droplets to Simulate Al_2O_3 Collision/Coalescence in Rocket Motors," *Journal of Propulsion and Power*, Vol. 7, No. 4, 1991, pp. 505–512.

[39]Pirumov, U. G., and Roslyakov, G. S., *Gas Flow in Nozzles*, Moscow State Univ., Russia, 1978, pp. 1–352.

[40]Sambamurthi, J. K., "Al_2O_3 Collection and Sizing from Solid Rocket Motor Plumes," *Journal of Propulsion and Power*, Vol. 12, No. 3, 1996, pp. 598–604.